buildings

MDPI

Article

Dynamic Response of Concrete Bridge Piers Under the Impact of Dry Granular Flow with Giant Boulders: A Scaled Model Study on the Force Mechanism of Boulders

Maili Cheng [1], Jutian Cheng [1,*], Pengpeng Ta [1], Xinjiang Chen [1], Shaoheng Guo [1,2] and Ye Zhang [1]

[1] School of Civil Engineering and Architecture, Yan'an University, Yan'an 716000, China; cheng_maili0610@yau.edu.cn (M.C.); tpp131452@163.com (P.T.); 19193756084@163.com (X.C.); gsh27407@163.com (S.G.); 19591153806@163.com (Y.Z.)
[2] Flood Control, Drought Relief and River-Lake Water Affairs Center of Alxa Left Banner, Alxa 750300, China
* Correspondence: cjt2446108718@163.com

Abstract

Dry granular flow disasters occur frequently in mountainous areas. The impact of dry granular flow with giant boulders poses a serious threat to the stability of concrete bridge piers. In this study, physical model tests were combined with PFC-FLAC coupled numerical simulations to investigate the dynamic response of concrete bridge piers under the impact of dry granular flow with giant boulders. The force model of the giant boulders considering the boulder size (S) and the distance in front of the slope (L) was analyzed. The proposed method was validated through a dual comparison of the peak acceleration at the pier top (with a relative error of 30%) and the macroscopic accumulation morphology. The results showed that the method can effectively simulate the impact process of dry granular flow with giant boulders on bridge piers. It provides methodological support for parametric studies of the pier impact response at different boulder sizes. The acceleration time histories and accumulation morphologies obtained from the numerical simulations agreed well with the test results. The peak impact force on the pier in the X direction first decreased and then increased with the increase in boulder size, and the peak impact force was 4.89×10^3 N when S = 15 cm. It first increased and then decreased with the increase in the distance in front of the slope; the peak impact force reached 5.04×10^2 N when L = 0.15 m, and the peak time was prolonged. The acceleration at the pier top increased with the increase in boulder size and decreased with the increase in the distance in front of the slope. The force analysis of the giant boulders indicated that the density of the dry granular flow and the boulder size are the key parameters controlling the forces acting on the boulders. The supporting force and the drag force increased with the increase in the density of the dry granular flow, and the friction force decreased with the increase in density. The gravity and the supporting force of the boulders increased with the increase in boulder size. This study reveals the influence laws of boulder size and the distance in front of the slope on the impact of dry granular flow on bridge piers. The findings can provide a theoretical basis for the impact-resistant design of bridges and disaster prevention in mountainous areas.

Keywords: dry granular flow; boulder size; distance in front of the slope; pier response; force analysis of giant boulders

Check for updates

Academic Editor: Salvatore Verre

Received: 24 September 2026
Revised: 15 October 2026
Accepted: 21 October 2026
Published: 23 October 2026

Copyright: © 2026 by the authors. Licensee MDPI, Basel, Switzerland. This article is an open access article distributed under the terms and conditions of the Creative Commons Attribution (CC BY) license.

1. Introduction

The impact of dry granular flow often causes severe damage to transportation infrastructure distributed in gullies and steep mountainous areas. Bridge piers are the key hazard-bearing bodies and are highly vulnerable to dry granular flow disasters [1]. In May 2026 alone, the Yacural Bridge in Iribarren, Lara State, Venezuela, and the Shibian Bridge in Yan'an, China, collapsed due to dry granular flow disasters, resulting in serious losses. Therefore, it is of great significance to investigate the disaster-causing mechanism of dry granular flow impacting bridges in mountainous areas.

The disaster-causing mechanism of dry granular flow impact is a core issue in the field of disaster prevention and mitigation [2]. Existing studies have been carried out mainly from three aspects: theoretical analysis, numerical simulation, and physical experiments. In terms of theoretical analysis, He et al. [3] established an impact force prediction model considering the components of debris flow based on the particle size distribution. They pointed out that the impact force of boulders is the largest among all the components. Yang et al. [4] established an impact dynamics model of debris flow containing boulders. They proposed a theoretical calculation formula considering the boulder diameter, mass, and impact velocity. Si et al. [5] introduced a shape coefficient and established a semi-theoretical impact force formula considering the boulder diameter and irregular shape. In terms of numerical simulation, Zhang et al. [6] studied the dynamic response of reinforced concrete bridge piers under the impact of dry granular flow based on a coupled smoothed particle hydrodynamics, discrete element method, and finite element method (SPH-DEM-FEM) model. Jiang et al. [7] analyzed the impact effect of debris flow and boulders on high-speed railway bridge piers using the SPH-FEM method. Jin et al. [8] investigated the impact of tsunami-induced debris flow on bridge piers using the CFD-DEM coupled method. Numerical methods can accurately reproduce the entire disaster process of dry granular flow from initiation to impact and accumulation [9]. However, their parameter calibration and model validation still rely on physical experiments. In terms of physical experiments, Xing et al. [10] studied the deformation and failure behavior of buildings under the impact of dry granular flow. Kim et al. [11] analyzed the influence of baffle arrays on the flow behavior and dynamic impact force of dry granular flow based on scaled tests. Yu et al. [12] revealed the laws of stress fluctuation and structural vibration when dry granular flow impacts cylindrical obstacles. Field monitoring is constrained by uncertain factors, and post-disaster data acquisition is extremely limited [13]. Therefore, physical model tests are still the key approach to reveal the impact mechanism and calibrate numerical parameters [14].

In terms of structural factors, the section shape of bridge piers has a significant influence on the impact response of dry granular flow. Circular sections are widely used in engineering practice, but not all bridge piers in actual bridge construction are circular. Cheng [15] compared the dynamic response of bridge piers with different section shapes based on a PFC numerical model. The results showed that rectangular piers have a higher obstruction efficiency. Wang et al. [16] analyzed the influence of section shape on the impact drag coefficient of debris flow using the CFD-DEM coupled method. They further compared circular and square piers and found that the drag coefficient of square piers (1.23) is significantly larger than that of circular piers (0.58) [17]. Liang et al. [18] showed that circular sections are more favorable for particle flow around the piers and energy dispersion. Existing studies have paid insufficient attention to rectangular section piers. Therefore, the dynamic response law of rectangular piers under the impact of dry granular flow needs further investigation.

In terms of medium factors, the particle size of dry granular flow is distributed over a wide range, from millimeter-scale fine particles to meter-scale giant boulders.

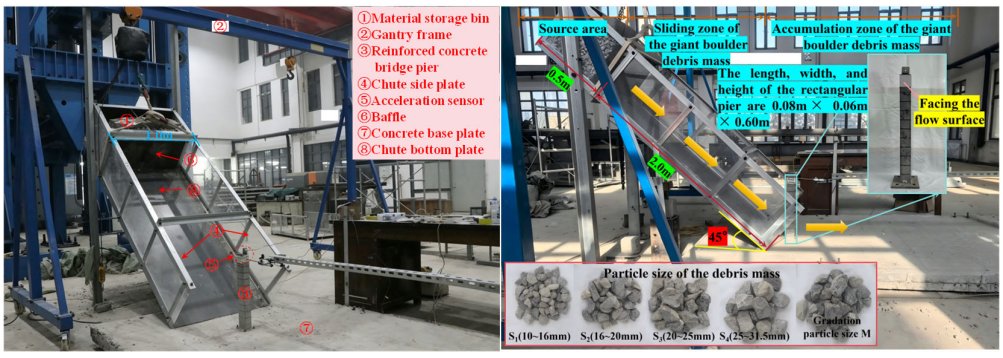
Tang et al. [19] analyzed the influence of dry granular flow with different particle sizes on the impact force and damage modes of bridge piers. Yao et al. [20] studied the collision mechanism between debris flow and bridge piers in the particle size range of 0.001 to 20 mm using the SPH-FEM adaptive coupled method. They found that the median particle size significantly affects the impact failure process. Wang et al. [21] revealed the coupling effect of particle size characteristics and flow conditions based on DEM simulations. Liu et al. [22] evaluated the impact damage of boulders with different particle sizes on check dams. However, the above studies mainly focused on dry granular flow in homogeneous and fine particle size ranges. The influence law of dry granular flow containing giant boulders on the dynamic response characteristics of bridge piers [23] still lacks in-depth investigation.

In view of this, the whole process of dry granular flow with giant boulders impacting concrete bridge piers was investigated in this study based on physical model tests and a PFC-FLAC coupled numerical model. This study focused on the evolution characteristics of the impact force time history and the dynamic response of bridge piers under different boulder sizes and distances in front of the slope. The agreement between the test results and the numerical simulation results was discussed, and the force analysis of the giant boulders was carried out. The findings can provide a theoretical basis for the impact-resistant design, safety assessment, and disaster prevention of bridges in mountainous areas.

2. Physical Model Test Setup and Materials

2.1. Test Setup

In this study, a physical model test platform for debris impact was designed and built, as shown in Figure 1. The test platform consists of a material storage bin, a flow-guiding chute, acceleration sensors with a sampling frequency of 1000 Hz, a rectangular pier model, and a concrete bearing base plate. It can be adapted to various model test studies on the impact of dry granular flow on structures. The chute is 2.5 m long, 1.0 m wide, and 0.5 m high. A material storage bin with a length of 0.5 m is set at the rear of the chute. The debris mass is released by pulling out the pin of the front baffle of the material bin. The sensors are installed at the top of the scaled pier to collect the acceleration time history data at the pier top in real time. Three high frame rate cameras (Canon EOS 80D digital camera (Canon Inc., Tokyo, Japan) with a resolution of 1920 × 1080) are arranged in the test area to synchronously record the whole process of initiation, impact, and accumulation of the dry granular flow.



(**a**) (**b**)

Figure 1. Impact test setup for dry granular flow with giant boulders: (**a**) 45° View of the impact test setup; (**b**) Side view of the impact test setup.

2.2. Test Materials

Considering the influence of the size effect of the debris mass [24,25], the diameter of the debris particles was set to be less than 1/20 of the chute width, and the side length

of the giant boulders was set to be less than 1/5 of the chute width. Accordingly, gravel with a particle size of 10 to 31.5 mm was selected to simulate the debris mass in the tests. The gravel was sieved into four particle size groups, namely S_1 (10 to 16 mm), S_2 (16 to 20 mm), S_3 (20 to 25 mm), and S_4 (25 to 31.5 mm). The four groups were mixed according to the mass proportions of 25%, 35%, 30%, and 10% to form the debris mass of gradation M. Concrete cubes with side lengths of 7 cm, 9 cm, 11 cm, 13 cm, and 15 cm were placed on the surface of the debris mass to simulate giant boulders of different sizes.

2.3. Pier Model

This study takes three engineering events as the engineering background. They are the dry granular flow disaster of a viaduct of the Lanzhou-Xinjiang High-Speed Railway in 2022 [26], the debris flow disaster of the Ortiano II Viaduct in Italy in 2023 [27], and the rockfall disaster of the Pescatore Viaduct in Italy in 2024 [28]. The piers in these cases are all of rectangular cross-section. Rectangular cross-sections are widely used in high-pier bridges in mountainous areas. In addition, rectangular piers have a relatively high retention efficiency and bear larger impact forces and internal forces, which is a relatively unfavorable loading condition. Therefore, taking rectangular piers as the research object can provide a reference on the safe side for engineering design. Accordingly, a single-column reinforced concrete rectangular pier is selected as the research object in this study. The prototype pier has a cross-section of 1.6 m × 1.2 m and a height of 12 m, and the reinforcement is arranged according to the General Code for Concrete Structures [29]. According to the similarity theory [30], the scale ratio is taken as 1:20. The model pier was cast with a concrete grade of C30. The model pier has a cross-section of 0.08 m × 0.06 m and a height of 0.60 m. The rectangular pier is longitudinally reinforced with four HRB400 steel bars with a diameter of 6 mm, and the longitudinal reinforcement ratio is 2.36%, which meets the requirements of the code [31]. The stirrups have a diameter of 2 mm. They are arranged around the longitudinal reinforcement with a spacing of 50 mm along the pier height.

2.4. Test Conditions

In this study, five boulder sizes (S) and five pier-to-slope distances (L) were taken as variables. The chute size, the inclination angle (45°), and the total volume of the material (0.21 m^3, including 0.01 m^3 of giant boulders) were kept constant. Nine test conditions were designed, as shown in Table 1. Conditions 2, 3, 4, and 5 were analyzed by numerical simulations due to considerations of test cost and material consumption, while the other conditions were investigated by physical model tests.

Table 1. Design of test conditions.

Test No.	Boulder Size (cm)	Boulder Volume (m^3)	Number of Boulders (Pieces)	Debris Volume (m^3)	Gradation of Debris Mass (mm)	Distance in Front of the Slope (m)	Chute Inclination Angle (°)
1	7	0.01	30	0.2	M	0.15	45
2	9	0.01	14	0.2	M	0.15	45
3	11	0.01	8	0.2	M	0.15	45
4	13	0.01	5	0.2	M	0.15	45
5	15	0.01	3	0.2	M	0.15	45
6	7	0.01	30	0.2	M	0.00	45
7	7	0.01	30	0.2	M	0.30	45
8	7	0.01	30	0.2	M	0.45	45
9	7	0.01	30	0.2	M	0.60	45

3. Coupled Numerical Model

Indoor model tests have the disadvantages of long duration, high cost, and low test efficiency. Therefore, a numerical simulation model was established and calibrated in this study based on the indoor model tests of dry granular flow with giant boulders impacting bridge piers. On this basis, numerical simulation studies of dry granular flow with giant boulders impacting bridge piers were carried out.

3.1. PFC-FLAC Coupled Simulation Method

In this study, the PFC-FLAC3D coupled method was adopted to simulate the dynamic response of bridge piers under the impact of dry granular flow with giant boulders. PFC is based on the discrete element theory. It describes the debris flow by tracking the movement of particles and the contact mechanical behavior between particles. The contact between particles adopts the rolling resistance linear model, and the contact force follows the force-displacement law (Figure 2a). FLAC3D is based on the finite difference method. It discretizes the continuum into hexahedral zones, which is suitable for simulating the continuum mechanical behavior of concrete bridge piers (Figure 2b). The two codes realize the force and displacement transfer between the discrete domain and the continuum domain through the wall-zone coupling scheme. At the coupling interface, the quadrilateral surface of a FLAC3D zone is automatically split into two triangular wall facets. The vertices of the facets coincide with the gridpoints of the zone, and their movement is driven by the displacement and velocity of the gridpoints. The contact force between the PFC particles and the wall facets is accordingly transferred to the structure (Figure 2c).

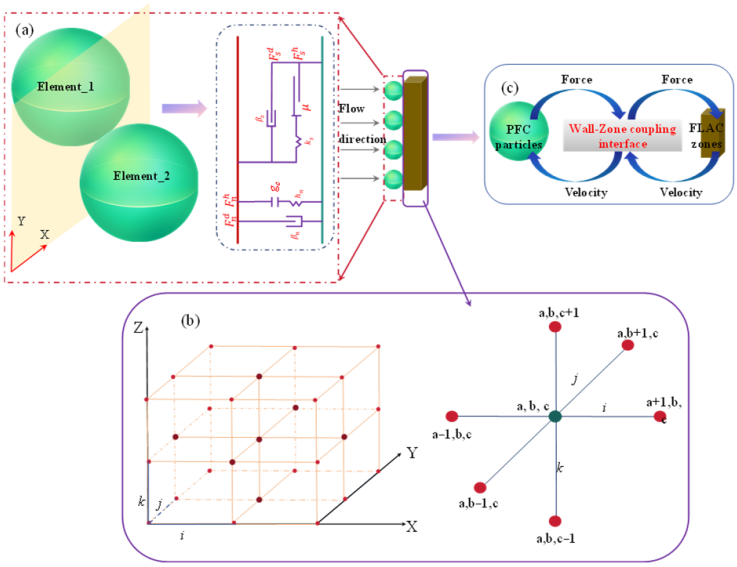


Figure 2. PFC-FLAC coupled model: (**a**) PFC discrete element contact model; (**b**) FLAC finite difference principle; (**c**) PFC-FLAC coupled calculation principle.

The coupling calculation was performed using PFC 9.0 and FLAC3D 9.0, and the model is three-dimensional. Both codes adopt the explicit central difference time integration. The two codes are advanced alternately, cycle by cycle, through the model cycle 1 command, so that the time steps remain synchronized. The coupled time step is taken as the smaller of the critical time steps of the two codes. The force and displacement information is exchanged once in every cycle. That is, the coupling frequency is $1/\Delta t$, where Δt is the time step. The coupled calculation proceeds step by step until the total calculation time reaches 4 s, thus completing the discrete-continuous coupled analysis. In FLAC3D, the pier is discretized into hexahedral brick zones.

When a particle is in contact with a facet, the contact force F is distributed to the three vertices of the facet by barycentric weighting. The weight of each vertex is

$$W_i = \frac{A_i}{A_0} \tag{1}$$

where W_i is the distribution weight of vertex i, which is a dimensionless proportional coefficient ($0 \leq W_i \leq 1$) and represents the fraction of the total contact force distributed to vertex i; A_0 is the total area of the triangular facet; A_i is determined as follows. The projection point CP of the contact point on the facet is connected to the three vertices, and the large triangle is thus divided into three small triangles. A_i is the area of the small triangle opposite to vertex i.

The equivalent force distributed to the node is

$$F_i = W_i F_0 \tag{2}$$

where F_0 is the total contact force between the particle and the facet, which is calculated by the contact constitutive model in PFC; F_i is the equivalent nodal force distributed to vertex i. Since $\Sigma W_i = 1$, the resultant force is strictly conserved during the distribution. The contribution of the contact stiffness is simultaneously transferred to the nodes to ensure numerical stability.

3.2. Establishment of the Numerical Model

A PFC-FLAC coupled numerical model of the physical model test was established at full scale (Figure 3). In PFC, the debris mass was simulated by ball elements, the giant boulders were simulated by rblock elements, and the chute and the concrete base plate were simulated by wall elements. In FLAC, the concrete bridge pier was simulated by zone elements, and the steel reinforcement was simulated by cable elements. The pier was discretized into 1200 hexahedral zone elements. The model contains 49,376 ball particles and 30 rblocks, and the time step is approximately 1.81×10^{-6} s. The concrete adopts the built-in plastic constitutive model in FLAC3D. In tension, the concrete undergoes strain softening after reaching the tensile strength, and a residual tensile stress is retained. In compression, the concrete first hardens to the peak value and then softens. During unloading, the concrete rebounds along the initial elastic path, and the stiffness degradation is not considered. The two-way transfer of displacement and force between the reinforcement and the concrete is realized through shape function interpolation. The interface is treated as fully bonded without slip. This constitutive model and the interface treatment have been verified through calibration, and they meet the accuracy requirements of the impact analysis.

3.3. Numerical Simulation Calibration

To ensure that the numerical model can reasonably reproduce the model test results, Condition 1 was taken as the calibration condition for parameter calibration. The parameters of this condition are as follows. The total volume of the giant boulders is 0.01 m^3, and the edge length of a single boulder is 7 cm. The debris mass adopts gradation M with a volume of 0.20 m^3. The distance in front of the slope is 0.15 m, and the inclination angle of the chute is 45°. The mesoscopic mechanical parameters of the reinforced concrete of the pier cannot be measured directly. Referring to the calibration method in reference [32], uniaxial compression tests were carried out on C30 concrete cubes of 150 mm × 150 mm × 150 mm. The parameter values were iteratively adjusted until the simulated uniaxial compressive stress–strain curve and the compressive strength agreed well with the test results (Figure 4). The calibrated mesoscopic mechanical parameters are listed in Table 2.

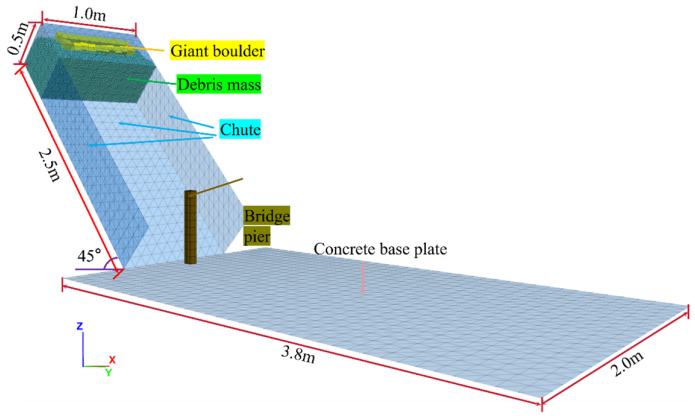


Figure 3. Numerical model of the impact between dry granular flow with giant boulders and bridge piers.

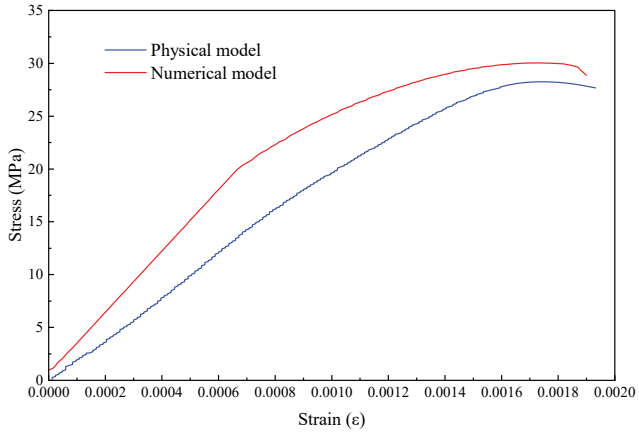


Figure 4. Comparison of the uniaxial compressive stress–strain curves of concrete.

Table 2. Meso-mechanical parameters of the reinforced concrete pier.

Meso-Mechanical Parameters of Concrete		**Mesoscopic Parameters of the Reinforced Concrete**	
Mechanical Property Parameters	**Numerical Value**	**Mechanical Property Parameters**	**Numerical Value**
Elastic modulus (Pa)	2.00×10^9	Density (kg/m^3)	7.85×10^3
Poisson's ratio	0.28	Cross-sectional area of reinforcement (mm^2)	28.27
Tensile strength (Pa)	3.48×10^6	Elastic modulus (Pa)	2.00×10^{10}
Compressive strength (Pa)	3.20×10^7	Tensile yield force (Pa)	4.00×10^8
Yield strength ratio	1.16		

The mesoscopic parameters of the numerical model were calibrated based on the test data of Condition 1. Figure 5 compares the acceleration time histories at the pier top. The simulated curve agrees well with the test curve in terms of the overall trend. The peak acceleration at the pier top is -1.08×10^2 m/s^2 in the test and -1.55×10^2 m/s^2 in the simulation. The relative error is approximately 30%, which is comparable to the error of 29.8% reported in reference [33] for similar model tests and numerical simulations. This indicates that the model is effective and reliable. The simulation also accurately captured the process at t = 1.50 s, in which the giant boulder impacted the upstream face of the pier and caused a sharp increase in the acceleration at the pier top. Although there is a certain deviation in the peak acceleration, the overall variation trend of the acceleration at the pier top is highly consistent, which verifies the capability of the model to simulate the impact dynamic response.

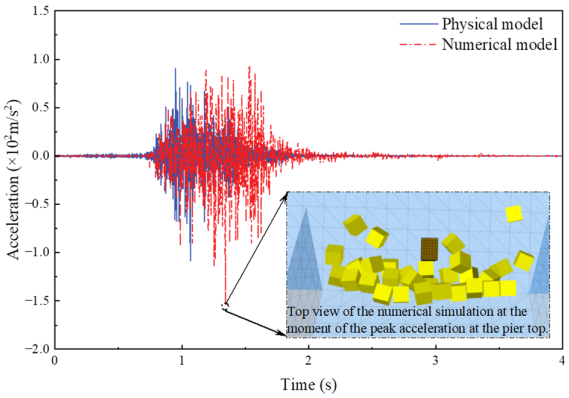


Figure 5. Comparison of the acceleration time history curves at the pier top.

Figure 6 shows the comparison of the accumulation morphology of the debris mass between the test and the numerical simulation under Condition 1. In the model test, square grids of 10 cm × 10 cm were arranged on the concrete base plate to quantify the accumulation range and planar morphology of the debris mass. The comparison between the test and the numerical simulation results shows the following. The accumulation lengths of the debris mass on the concrete base plate were 100 cm and 97 cm, with a relative error of 3.0%. The accumulation widths were 146 cm and 148 cm, with a relative error of 1.4%. The accumulation heights in front of the pier were 26 cm and 28 cm, with a relative error of 7.7%. The accumulation heights behind the pier were 20.5 cm and 22 cm, with a relative error of 7.3%. The relative errors of all the accumulation characteristic parameters are within 8%. The accumulation morphology obtained from the numerical simulation agrees well with the test results. This indicates that the numerical model can reasonably reproduce the accumulation characteristics of dry granular flow with giant boulders in the physical model test.

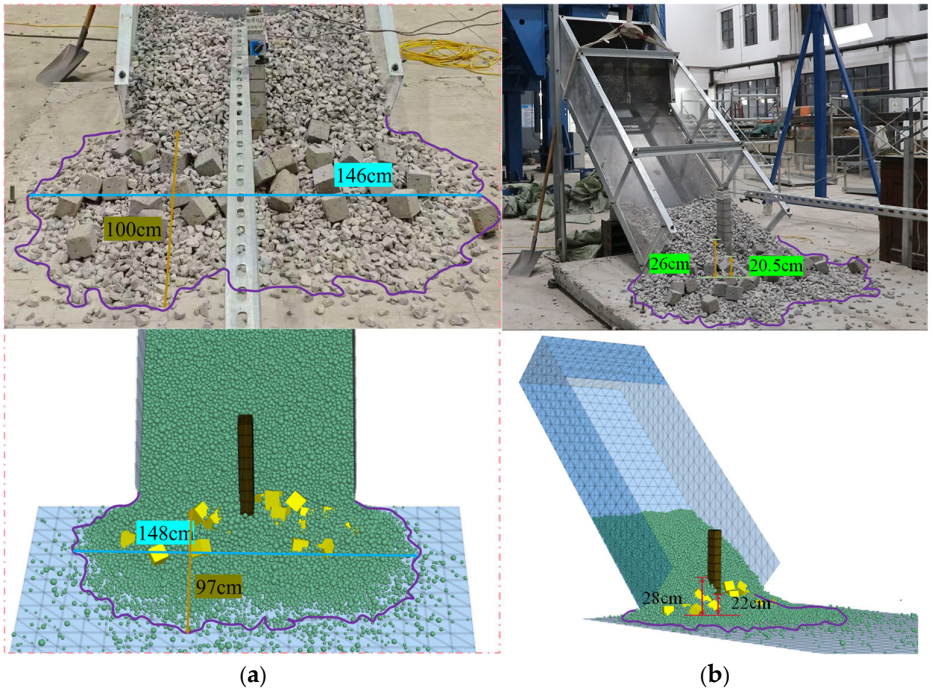


Figure 6. Accumulation morphology of the giant boulder debris mass: (**a**) front view; (**b**) isometric side view.

In the PFC model, based on references [9,15], the density of the giant boulders was set to 2.4 × 10^3 kg/m^3, and the global damping coefficient was set to 0.30. The density of the debris mass was set to 2.6 × 10^3 kg/m^3, the global damping coefficient was set to 0.10, and the porosity was set to 0.16. The other contact parameters are shown in Table 3, and their values were calibrated by the following steps. Condition 1 was taken as the baseline condition. The initial values of the static friction coefficient and the rolling friction coefficient were determined by referring to similar discrete element studies on rock and soil materials. Then, the dynamic response at the pier top and the accumulation morphology obtained from the numerical simulation were compared with those from the model test (Figures 5 and 6). The parameters were adjusted repeatedly until the two results agreed well. Based on this, the contact parameters of the giant boulder debris mass, the chute, and the concrete base plate were determined. The comparison results show that the calibrated model can well reproduce the movement morphology of the debris flow and the impact response of the pier under the baseline condition, and the calibration accuracy meets the research requirements. It should be noted that this comparison is a check of the calibration effect and does not constitute a model validation under independent loading conditions.

Table 3. Meso contact parameters of the PFC model.

Contact Materials	Contact Parameters			
	Effective Modulus (Pa)	Static Friction Coefficient	Rolling Friction Coefficient	Stiffness Ratio
Debris mass and debris mass	7.3 × 10^6	0.40	0.25	0.26
Giant boulder and giant boulder	1.0 × 10^6	0.20	0.12	0.2
Giant boulder and chute side plate	1.7 × 10^6	0.10	0.03	0.23
Giant boulder and chute bottom plate	1.5 × 10^6	0.15	0.10	0.22
Giant boulder and concrete base plate/pier	1.3 × 10^6	0.20	0.13	0.21
Debris mass and chute side plate	7.0 × 10^6	0.05	0.02	0.22
Debris mass and chute bottom plate	8.6 × 10^6	0.35	0.20	0.35
Debris mass and concrete base plate/pier	7.4 × 10^6	0.20	0.10	0.32
Debris mass and giant boulder	1.0 × 10^6	0.20	0.08	0.22

In this study, the rolling resistance linear contact model was adopted. The input parameters of this model are the elastic modulus and the stiffness ratio. The normal stiffness and the tangential stiffness are not input directly, and they are automatically calculated by the built-in formulation of PFC based on the above two parameters. When two particles are in contact, the normal stiffness is calculated as follows:

$$k_n = \frac{Ed^e}{1 - v^2} \tag{3}$$

where k_n is the normal stiffness; E is the elastic modulus of the particles; v is the Poisson's ratio of the particles; d^e is the equivalent diameter of the two contacting particles.

When a particle is in contact with a wall, the normal stiffness is calculated as follows:

$$k_n = 2E^e d_3 \tag{4}$$

where E^e is the equivalent elastic modulus of the contact between the particle and the wall; d_3 is the diameter of the single particle.

The ratio of the tangential stiffness to the normal stiffness, referred to as the stiffness ratio, is calculated as follows:

$$\lambda = \frac{k_s}{k_n} \tag{5}$$

where λ is the stiffness ratio; k_s is the tangential stiffness.

4. Dynamic Response Analysis of Bridge Piers Under the Impact of Dry Granular Flow with Giant Boulders

4.1. Analysis of the Acceleration Response at the Pier Top

This study adopted a hybrid method combining numerical simulation and physical model tests. The numerical simulations of Conditions 1 to 5 were used to study the response laws of the acceleration at the pier top under different boulder sizes. The physical model tests of Conditions 1 and 6 to 9 were used to compare and analyze the response laws of the acceleration at the pier top under different distances in front of the slope. Condition 1 was the common baseline condition of the two series. The comparison of the relative errors between the numerical simulation and the physical test results verified the consistency of the two methods. This ensures a unified comparison baseline for each series, and the two series are connected through the baseline condition.

4.1.1. Influence of Boulder Size on the Acceleration at the Pier Top

Figure 7 shows the time history curves of the acceleration at the pier top under the impact of the dry granular flow with giant boulders under Conditions 1–5. It can be seen that the acceleration at the pier top increases with the increase in the boulder size S. When the total volume of the giant boulders is constant, the number of giant boulders decreases with the increase in S, and the number of collisions between particles and the energy consumption during the sliding process are reduced. When 7 cm $\leq S \leq$ 9 cm, the load of the giant boulders is dispersed and the pier is impacted at multiple positions; when S > 9 cm, the number of giant boulders decreases and the dry granular flow tends to impact the pier as a single body, leading to a sharp increase in the pier-top acceleration. When S = 15 cm, the peak acceleration at the pier top reaches 1.10×10^3 m/s^2. In addition, the differences in the shapes of the acceleration time histories among the cases are also related to the randomness of boulder motion. Due to kinetic sieving, the boulders migrate to the surface of the granular flow and undergo random rolling and sliding, and random collisions change the impact angle and the number of impacts on the pier. Nevertheless, the law that the pier-top acceleration increases with boulder size is consistent across all cases and is statistically robust; the quantitative influence of this randomness will be further verified through repeated tests in future work.

4.1.2. Influence of the Distance in Front of the Slope on the Acceleration at the Pier Top

Figure 8 shows the time history curves of the acceleration at the pier top under the impact of dry granular flow with giant boulders at S = 7 cm for L = 0.00 m, L = 0.15 m, L = 0.30 m, L = 0.45 m, and L = 0.60 m. The analysis of Figure 8 shows that the acceleration at the pier top decreases with the increase in the distance in front of the slope. After the dry granular flow with giant boulders rushes out of the chute, the sliding friction between the dry granular flow and the concrete base plate and the collisions between the particles continuously consume the kinetic energy of the dry granular flow as the distance in front of the slope increases. The lateral spreading range of the dry granular flow on the concrete base plate increases with the increase in the distance in front of the slope. Thus, the interception efficiency of the upstream face of the pier on the dry granular flow decreases, and the unit impact force of the dry granular flow on the pier decreases. As the distance in front of the slope increases, the particles at the front edge of the dry granular flow form a buffer layer in front of the upstream face of the pier. The buffer layer obstructs the particles at the rear edge and dissipates energy. However, it should be noted that when L = 0.30 m, the pier did not cause a blocking and energy dissipation effect on the dry granular flow at

the slope toe. The energy dissipation of the dry granular flow due to the distance in front of the slope was small, and the giant boulders retained a large amount of kinetic energy. One giant boulder directly hit the upstream face of the pier. Therefore, the peak acceleration at the pier top increased slightly.

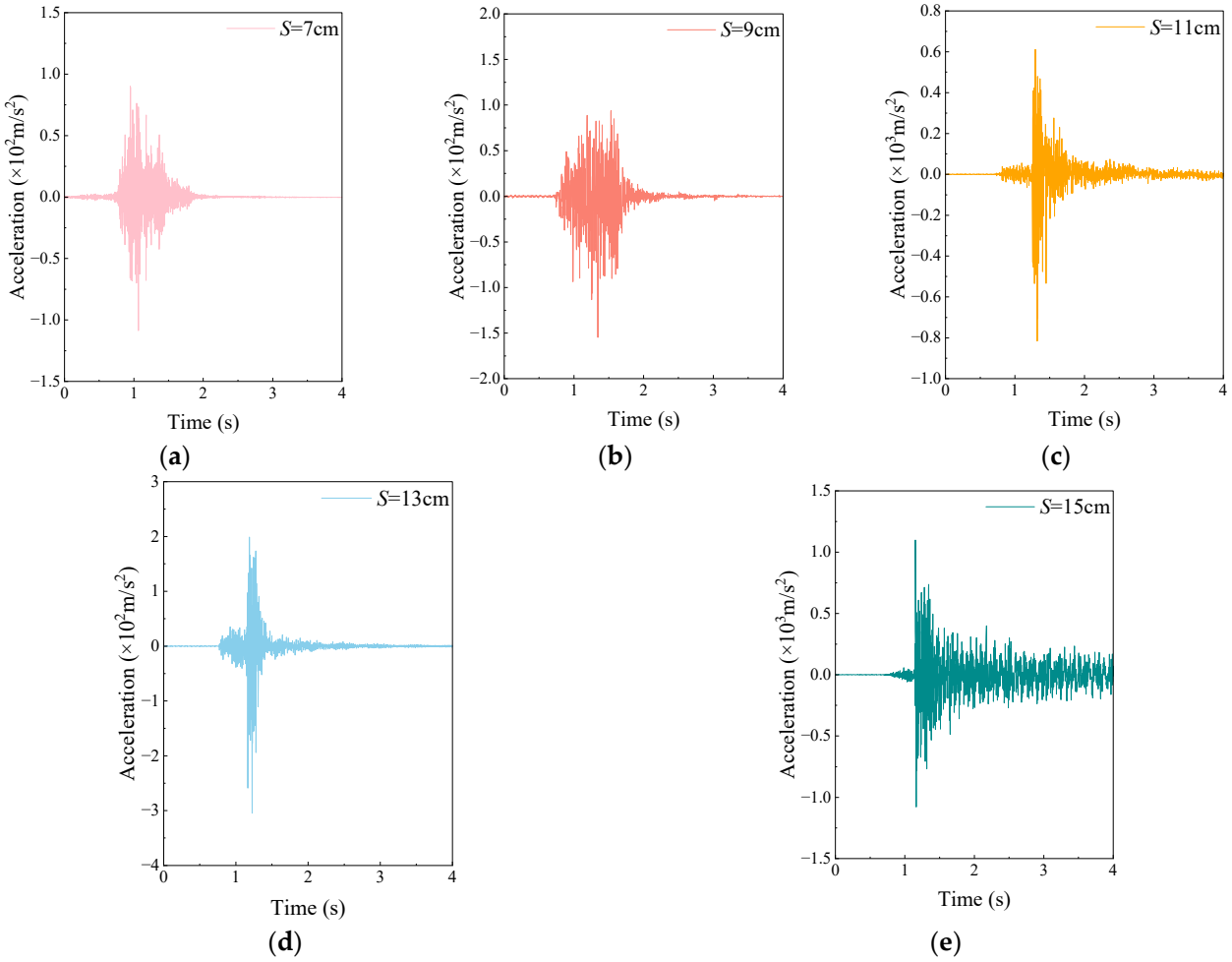


Figure 7. Influence of boulder size on the acceleration at the pier top: (**a**) S = 7 cm; (**b**) S = 9 cm; (**c**) S = 11 cm; (**d**) S = 13 cm; (**e**) S = 15 cm.

The accelerations reported herein are the pier-top accelerations, which characterize the global dynamic response of the pier structure under collision, rather than the local response of the contact zone. The relatively high acceleration magnitude can be attributed to the following aspects: the collision contact lasts only at the millisecond level, and the sudden change in momentum produces a large instantaneous impact force; under impact excitation, the stiffer the structure, the more significant its acceleration response, and the pier top is exactly the location where the first-mode response of the cantilever pier reaches its maximum; the particles in the scaled model have small sizes and high contact stiffness, resulting in relatively high peak impact forces. Moreover, the test follows the Froude similarity criterion, under which the acceleration scale ratio is unity, meaning that the scaling process does not amplify the acceleration; therefore, the measured high accelerations are consistent with the actual response magnitude of the prototype structure and are physically realistic. However, it should be noted that the test specimen is a scaled model of a single pier component, which differs significantly from actual bridge structural systems; therefore, the test results cannot be directly used for engineering analysis and design. This study aims to reveal the dynamic response laws of the structure under impact,

which still need to be converted through similarity relations and further verified by full-bridge model tests or numerical simulations.

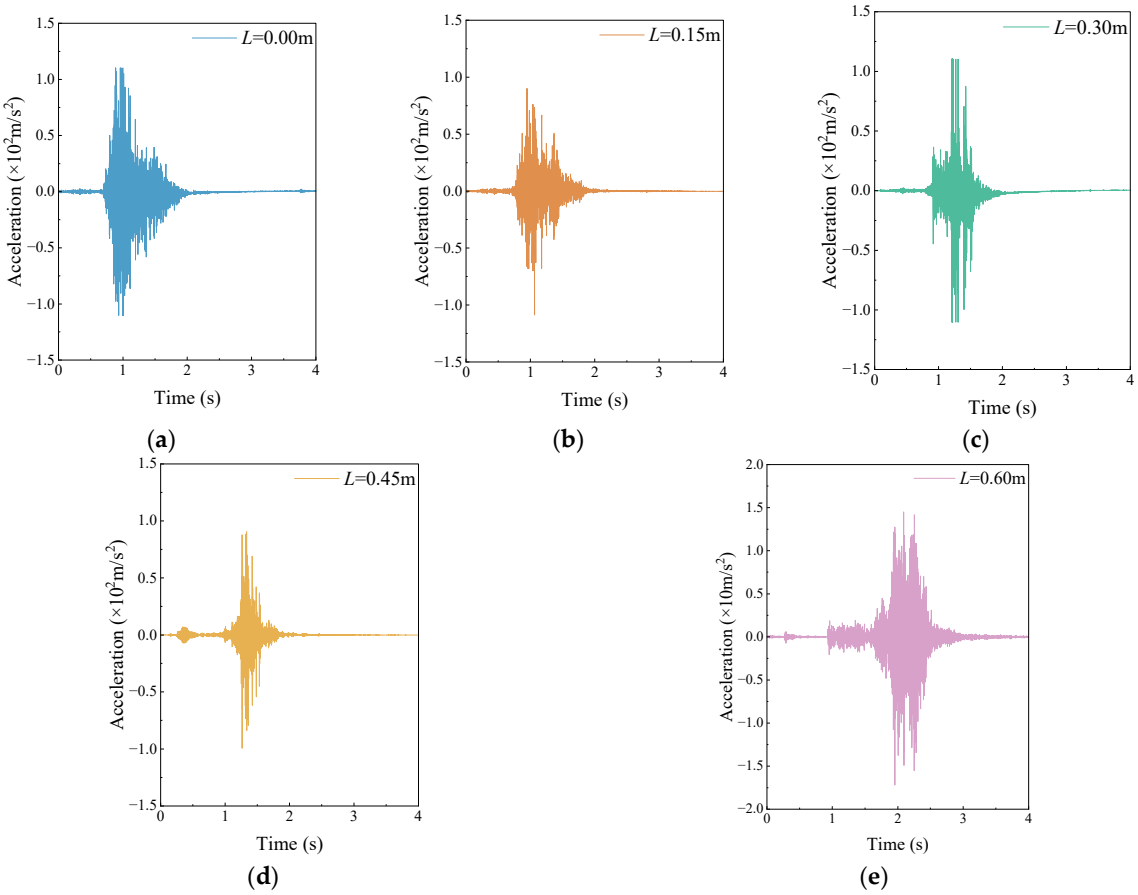


Figure 8. Influence of the distance in front of the slope on the acceleration at the pier top: (**a**) L = 0.00 m; (**b**) L = 0.15 m; (**c**) L = 0.30 m; (**d**) L = 0.45 m; (**e**) L = 0.60 m.

4.2. Analysis of the Impact Force of Dry Granular Flow with Giant Boulders

The impact force of the dry granular flow decays along the pier height, and the impact of particles in the region above 0.40 m from the pier bottom is very rare [9]. Accordingly, monitoring grids for the impact force were arranged within 0.00–0.40 m from the pier bottom, and the distribution characteristics of the impact force along the pier height were analyzed based on the numerical simulation results.

4.2.1. Distribution Characteristics of the Horizontal Impact Force

Figure 9 shows the time history curves of the horizontal impact forces in the X and Y directions of the pier under the impact of dry granular flow with giant boulders for Condition 1. As shown in Figure 9, the time history of the impact force can be divided into four stages, namely the initiation and collapse stage, the impact rising stage, the congestion and deceleration stage, and the stopping and accumulation stage. In the initiation and collapse stage (0 to 0.74 s), the particles at the front edge of the debris mass had not reached the upstream face of the pier, and the impact forces in the X and Y directions were both 0. In the impact rising stage (0.74 to 1.50 s), the debris mass began to impact the pier after t > 0.74 s, and the impact forces in the X and Y directions increased sharply. At t = 1.50 s, a single giant boulder directly impacted the upstream face of the pier. The peak impact force in the X direction reached 5.04 × 10^2 N, and the peak impact force in the Y direction reached 1.22 × 10^2 N. In the congestion and deceleration stage (1.50 to 3.00 s), the particles

at the front edge accumulated around the pier and formed a buffer layer. The buffer layer obstructed the particles at the rear edge. The impact kinetic energy of the particles at the rear edge decreased when they moved to the pier. The force on the pier gradually changed from collision impact to static pushing. In the stopping and accumulation stage (3.00 to 4.00 s), the rolling and collision of a small number of particles caused small fluctuations in the impact force. The action of the accumulation body in front of the pier on the pier was mainly static lateral pressure. The dry granular flow with giant boulders moved along the chute in the X direction, and the kinetic energy mainly acted on the pier in the X direction. The impact force in the Y direction only came from the lateral action generated by the flow around the pier and the deflected collisions of a small number of particles. The residual impact force in the Y direction tended to 0. This indicates that there was no continuous pushing action in the Y direction after the accumulation became stable. Therefore, the impact force in the X direction was much larger than that in the Y direction. Based on this, this study focuses on the influence laws of the impact force in the X direction of dry granular flow with giant boulders on bridge piers.

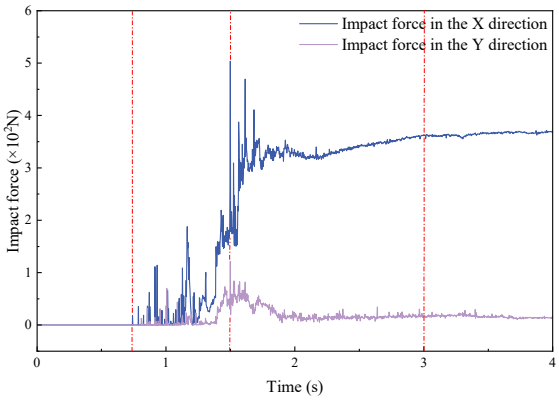


Figure 9. Time history curves of the horizontal impact forces on the pier in the X and Y directions.

4.2.2. Influence of Boulder Size on the Impact Force of the Pier in the X Direction

Figure 10 shows the time history curves of the impact force in the X direction exerted by the dry granular flow with giant boulders on the pier under Conditions 1–5. It can be seen that the boulder size S significantly affects the peak impact force in the X direction. The peak value first decreases and then increases with the increase in S. This non-monotonic law originates from the competition between the debris buffering and energy dissipation mechanism and the inertial impact mechanism of the giant boulders as the boulder size changes. The two mechanisms switch at the critical size S = 9 cm. When 7 cm $\leq S \leq$ 9 cm, the buffering and energy dissipation mechanism is dominant. When the total volume of the giant boulders is constant, a smaller size means a larger number of boulders, and the debris mass is dispersed in the gaps and can hardly form a continuous buffering structure. As S increases, the number of giant boulders decreases and the gaps are integrated and enlarged. More debris mass fills the gaps between the giant boulders and forms a continuous granular damping buffer layer in front of each giant boulder. During the impact, the kinetic energy of the giant boulders is first transferred to the debris mass in front of them. The energy is then converted into heat energy and deformation energy through particle sliding and extrusion friction, thus realizing graded dissipation. The buffered debris mass acts on the pier as a distributed load, and the direct rigid collision between the giant boulders and the pier is avoided. In this stage, the improvement in the energy dissipation efficiency of the buffer layer exceeds the inertia increment of the giant boulders. Therefore, the peak impact force decreases with the increase in S. When 9 cm < $S \leq$ 15 cm, the inertial impact mechanism becomes dominant. At this time, the contact area and the compressible space

of the buffer layer have reached the limit, and the energy dissipation capacity is saturated. However, the inertial momentum of the giant boulders increases significantly with the boulder size. The kinetic energy exceeds the dissipation threshold of the buffer layer, and the giant boulders break through the buffer layer and directly impact the pier in the form of quasi-rigid bodies. The impact mode changes from a distributed load to a concentrated block impact. The contact area becomes more concentrated and the local impulse density becomes higher. Therefore, the peak impact force increases monotonically with the increase in S.

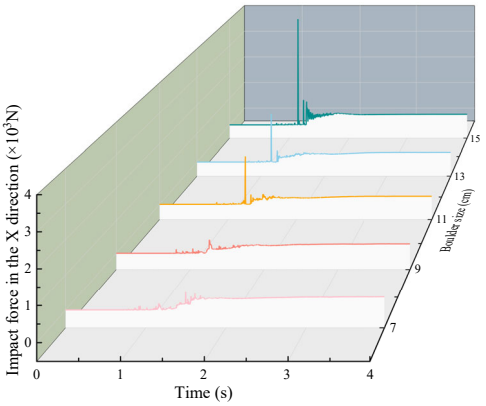


Figure 10. Influence of boulder size on the impact force of the pier in the X direction.

4.2.3. Influence of the Distance in Front of the Slope on the Impact Force of the Pier in the X Direction

Figure 11 shows the time history curves of the impact force in the X direction under the conditions of S = 7 cm and L = 0.00–0.60 m. It can be seen that with the increase in L, the impact force in the X direction first increases and then decreases, and the occurrence time of the peak value is continuously delayed. This non-monotonic law is jointly controlled by the frontal accumulation buffering effect, the velocity development effect of the granular flow, and the energy attenuation effect along the flow path. The dominant mechanism changes twice with the increase in L. When 0.00 m $\leq L \leq$ 0.15 m, the weakening of the buffering effect and the full development of the flow velocity jointly lead to an increase in the impact force. When L = 0.00 m, the pier is close to the chute outlet. The lateral constraint of the chute walls limits the lateral diffusion of the granular flow. The front particles are blocked by the pier and accumulate rapidly to form a buffer cushion layer. The impact kinetic energy of the subsequent particles is largely dissipated through collision and friction in the buffer layer before being transferred to the pier. Therefore, the initial peak impact force is relatively low. When L increases to 0.15 m, the granular flow escapes from the constraint of the chute outlet and obtains free space for development. A continuous accumulation body has not yet formed at the front, and the buffering effect basically disappears. Meanwhile, the velocity and the flow regime of the granular flow are fully developed, so the impact force reaches its maximum value. When L > 0.15 m, the energy dissipation along the flow path is dominant, and the impact force decreases continuously. As L further increases, the collisions between particles and the friction between the particles and the base plate continuously dissipate the kinetic energy, and the front velocity decays continuously. At the same time, the lateral diffusion of the granular flow is intensified. The proportion of the particle mass intercepted by the upstream face of the pier decreases, and the effective impact load is reduced. In this stage, the energy dissipation along the flow path and the diffusion effect play a controlling role. Therefore, the peak impact force decreases continuously with the increase in L.

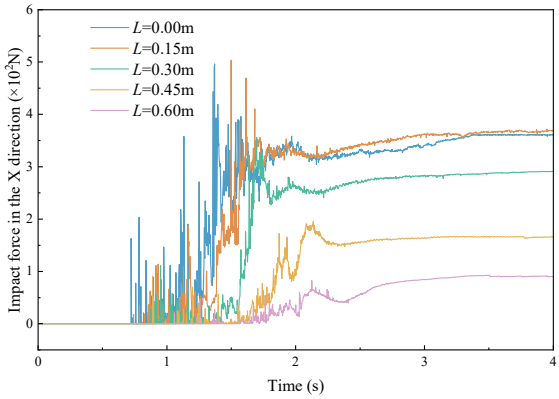


Figure 11. Influence of the distance in front of the slope on the impact force of the pier in the X direction.

Based on the Froude similarity criterion, the test results can be converted to the prototype. The geometric scale ratio is 1:20, and the material densities are similar. The scale ratio of the impact force is 1:8000. The peak impact force of the model (on the order of 10^2 N) can be converted to the order of 10^5 to 10^6 N for the prototype, which is basically consistent with the engineering range of the debris flow impact load on bridges in mountainous areas. The variation law of the impact force with the distance in front of the slope can provide guidance for bridge site selection and protection design. The converted magnitude can be used as a load reference for impact-resistant design. The above conversion is a theoretical estimation, and the practical application should be verified in combination with field conditions.

4.3. Force Analysis of Giant Boulders

Scholars at home and abroad have carried out extensive research on the forces acting on giant boulders in dry granular flow. Existing studies and the test results of this study both show that giant boulders have a significant influence on the peak acceleration and peak displacement at the pier top. Therefore, the force characteristics of the giant boulders are analyzed in this section. In this test, the giant boulders in the source area were submerged in the debris mass. Referring to the treatment methods of existing studies, the force process of the giant boulders was divided into four stages according to the motion state of the dry granular flow with giant boulders. The four stages are the incubation and initiation stage, the entrainment and transport stage, the impact and disaster-causing stage, and the stopping and accumulation stage. The force diagram of the giant boulders is shown in Figure 12.

Figure 12a shows the force state of the giant boulders in the incubation and initiation stage of the dry granular flow with giant boulders. In this stage, the giant boulders are mainly subjected to the supporting force F_N from the chute bottom plate, the gravity F_G, the extrusion force F_e of the debris mass, the drag force F_L, and the friction force F_s. Based on this, the force equilibrium equation of the giant boulders was established. The calculation formula of the friction force F_s is as follows:

$$F_s \leq \mu_s m_s g_r \cos\theta + F_e \tag{6}$$

where θ is the inclination angle of the chute; μ_s is the static friction coefficient; m_s is the mass of the boulder; g_r is the gravitational acceleration, taken as 9.8 m/s^2.

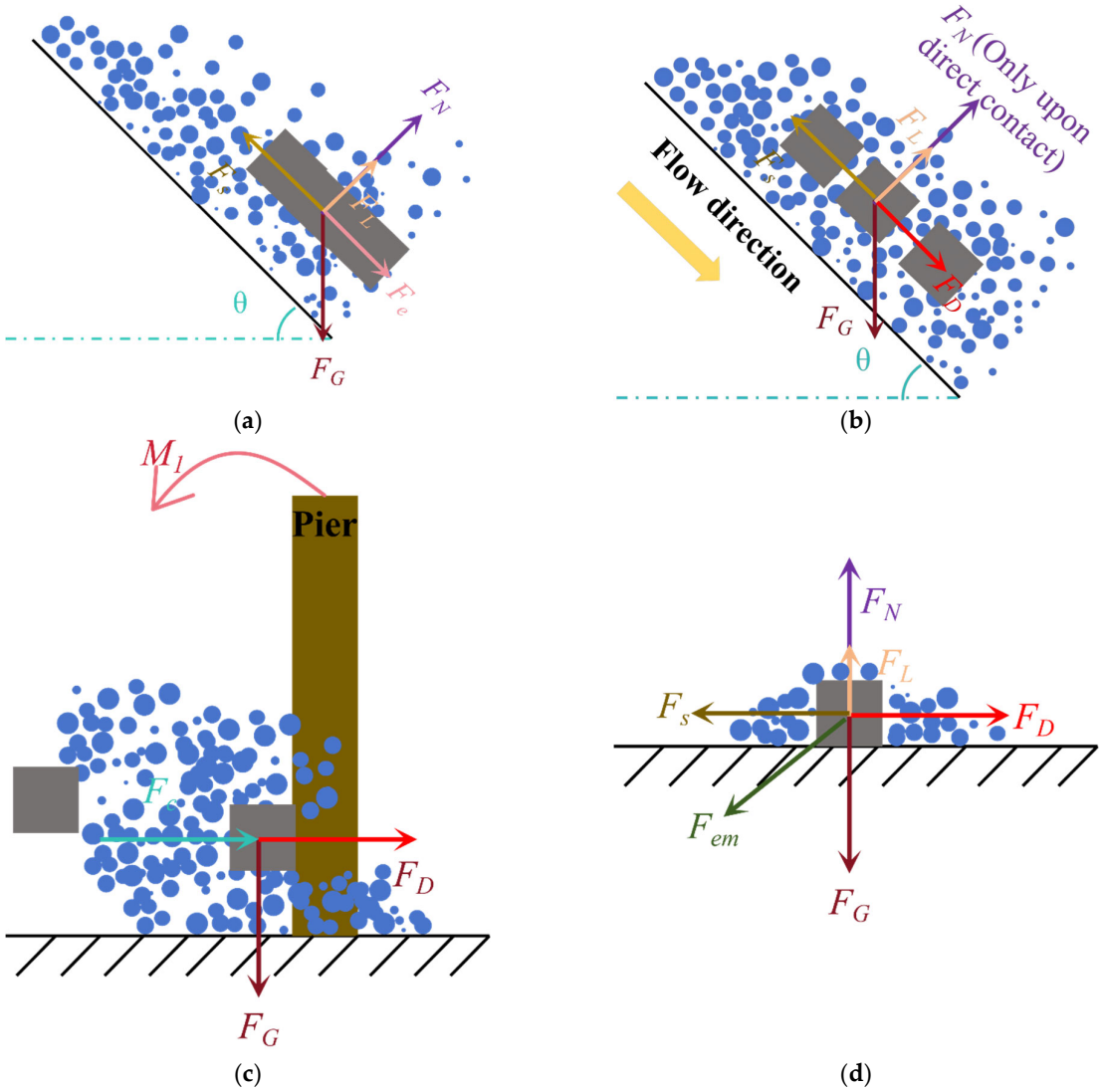


Figure 12. Force diagram of the giant boulders: (**a**) incubation and initiation; (**b**) entrainment and transport; (**c**) impact and disaster causing; (**d**) stopping and accumulation.

Figure 12b shows the force state of the giant boulders in the entrainment and transport stage of the dry granular flow with giant boulders. In this stage, the giant boulders are mainly subjected to the supporting force F_N from the chute bottom plate, the gravity F_G, the drag force F_D of the debris mass, the supporting force F_L from the dry granular flow, and the friction force F_s. The supporting force of the chute bottom plate is a contact force. It is generated only when the giant boulders compress the underlying debris mass during the movement and the bottom of the giant boulders is in direct contact with the chute bottom plate. Based on this, the force equilibrium equation of the giant boulders was established. The calculation formula of the supporting force of the dry granular flow on the giant boulders is as follows:

$$F_L = \rho_c g V_L \tag{7}$$

where ρ_c is the density of the dry granular flow (kg/m^3); V_L is the volume of the giant boulder submerged in the dry granular flow; g is the gravitational acceleration, taken as 9.8 m/s^2.

When part of the particles of the dry granular flow pass around the giant boulder, the giant boulder is subjected to the drag force F_D. The calculation formula is as follows:

$$F_D = \frac{1}{2}\rho_c A_d C_d \mu_{rel}^2 \tag{8}$$

where A_d is the action area of the drag force; C_d is the drag coefficient; ${\mu^2}_{rel}$ is the relative velocity between the giant boulder and the dry granular flow.

Figure 12c shows the force state of the giant boulder in the impact and disaster-causing stage of the dry granular flow with giant boulders. In this stage, the giant boulder is mainly subjected to the gravity F_G, the drag force F_D of the debris mass, the impact force F_c of the giant boulder, and the rotational moment M_1. Based on this, the force equilibrium equation of the giant boulder was established. The giant boulder collides with the pier. In this study, the giant boulder and the pier are simplified as rigid bodies. According to the theorem of rigid body dynamics, the moment equation M_1 of the giant boulder is as follows:

$$M_1 = m_s e \frac{\Delta V}{\Delta T} \tag{9}$$

where e is the eccentric distance from the action line of the collision force to the mass center of the giant boulder, with a value range of $0 \leq e \leq R$ referring to reference [34], where R is the radius of the giant boulder; ΔV is the velocity change in the giant boulder before and after the collision with the pier; and ΔT is the contact duration of the collision between the giant boulder and the pier.

Figure 12d shows the force state of the giant boulder in the stopping and accumulation stage of the dry granular flow with giant boulders. In this stage, the giant boulder is mainly subjected to the supporting force F_N from the concrete base plate, the gravity F_G, the drag force F_D of the debris mass, the supporting force F_L, the embedding force F_{em} of the debris mass on the giant boulder, and the friction force F_s. Based on this, the force equilibrium equation of the giant boulder was established. The termination condition of the movement of the giant boulder is as follows:

$$F_D \leq \mu(m_s g - F_L - F_N) + F_{em} \tag{10}$$

From the above four-stage force analysis of the giant boulder, it can be seen that under the condition of constant boulder size, the supporting force and the drag force of the dry granular flow on the giant boulder increase with the increase in the density of the dry granular flow, while the friction force decreases with the increase in the density of the dry granular flow. Under the condition of constant density of the dry granular flow, the gravity and the supporting force of the giant boulder increase with the increase in boulder size, and the friction force is determined by the difference between the gravity and the supporting force of the giant boulder.

5. Discussion

Under extreme climate conditions, the particle distribution and migration process of rock avalanche dry granular flow have great uncertainty. The particle composition of the rock avalanche debris mass, the complexity of the surface morphology of the slope, and the action of earthquakes can reduce the friction force and interlocking force between the debris particles. These factors can increase the risk of rock mass collapse and prolong the migration distance of the rock avalanche dry granular flow. During the process of slope instability, the loose rock mass transforms into dry granular flow through sliding and

collapse. The dry granular flow can easily entrain giant boulders to move together during the migration process.

It is worth noting that there is a certain difference between the numerical simulation results and the test results of the peak acceleration at the pier top, with a relative error of about 30%. This difference mainly originates from the inherent limitations of the test measurement system. In the test, the acceleration sensor was limited by the sampling frequency, and the true peak value and its occurrence time were difficult to be completely captured. As a result, the measured value is systematically lower. In the numerical simulation, the monitoring point was set directly at the pier top and vibrated completely synchronously with the pier, so the simulated peak value is relatively larger. In view of this, the sampling frequency can be increased and multi-channel synchronous acquisition can be adopted in future studies to ensure the complete recording of the true peak value. The measurement boundary consistent with the test can be reproduced in the numerical simulation, such as by establishing a model of the bracket system, so as to achieve a stricter comparison and verification between the simulation and the test.

Existing studies have shown that the increase in particle size in dry granular flow increases the impact force and its peak value. This means that giant boulders have stronger energy transfer capacity and destructiveness when impacting bridge piers. Figure 10 further shows that the impact force of dry granular flow with giant boulders shows an overall upward trend with the increase in boulder size, and the increase in the amplitude of the peak impact force is significant. This indicates that the increase in boulder size within a certain range can enhance the instantaneous impact action of dry granular flow with giant boulders. From the perspective of the motion mechanism, the giant boulders have large mass and high inertia. They can maintain high kinetic energy during high-speed movement and produce large local concentrated loads when impacting the pier. Meanwhile, the debris mass forms stable force chain transmission during the movement of the dry granular flow. The energy loss of the giant boulders is small. Due to the inertia effect, the impact contact time is shortened, the energy transfer efficiency is improved, and the impact impulse increases. Therefore, the direct impact of the giant boulders may control the local peak force of the pier and become an important inducing factor for the damage and even failure of the pier structure.

The distance in front of the slope is an important factor affecting the dynamic response of bridge piers. Figure 8 shows that the peak acceleration at the pier top is the largest when L = 0.30 m. Figure 11 shows that the peak impact force of the dry granular flow with giant boulders on the pier is the largest when L = 0.15 m. The distances in front of the slope corresponding to the peak values of the two indicators are not consistent, and neither indicator decreases monotonically with the increase in the distance in front of the slope within the range of the conditions in this study. This indicates that the dynamic response of the pier is relatively large and the layout position is relatively unfavorable when L is within 0.15–0.30 m. It should be pointed out that this conclusion is based on limited configurations, and no structural damage criterion is introduced. Therefore, it is not sufficient to serve as a universal determination of the most dangerous interval. More general quantitative relationships remain to be studied with more configurations and damage indicators. In addition, although the increase in the distance in front of the slope increases the movement path of the granular flow, the pier may still bear strong instantaneous impact loads. Therefore, the impact resistance requirements of the pier should not be relaxed in engineering design due to the increase in the distance in front of the slope.

This non-monotonic behavior can be explained by the competition between energy dissipation and flow accumulation effects. On the one hand, the increase in the distance in

front of the slope extends the movement path of the granular flow, and more kinetic energy is dissipated through inter-particle friction and particle-ground friction, which reduces the impact velocity and tends to weaken the impact response. On the other hand, the granular flow diffuses laterally and accumulates gradually after leaving the channel, resulting in an increase in effective impact area and impact depth on the pier. For the flow with giant boulders, the velocity of boulders attenuates much slower than fine particles during rolling, so the growth rate of impact area exceeds the attenuation rate of kinetic energy. The trade-off between these two effects leads to the non-monotonic variation in impact acceleration and force, which means the pier can still be subjected to severe instantaneous impact loads at a larger slope front distance.

Limited by the cost and site conditions of large-scale impact tests, and considering that the debris flow has strong discreteness and the initial conditions are difficult to keep completely consistent, only one valid test was carried out for each condition. The results are single measurements rather than statistical averages, which is consistent with the common practice of large-scale geotechnical dynamic model tests. To ensure the reliability of the data, the measurement system was uniformly calibrated before the tests, and the gradation, filling, and initial accumulation morphology were strictly controlled during the tests. The obtained laws agreed well with the numerical simulation results (Figures 6 and 7). However, a single measurement cannot evaluate the discreteness and the confidence interval. Meanwhile, limited by the computing power and test conditions, only the parameter calibration of the baseline condition has been completed at present. The distance series still lacks independent numerical validation, and the conditions with large boulder sizes are numerical predictions. In future studies, multiple batches of repeated tests will be carried out to improve the statistical significance. Independent simulations of all the conditions of the distance series will be supplemented, and physical model tests with large boulders will be gradually carried out, so as to further improve the applicability of the model and the reliability of the conclusions.

The force analysis of the giant boulders in this study is established based on the critical condition of instability initiation, which is a theoretical approximation. The actual movement of the dry granular flow with giant boulders is complex. The directions of the drag force and the embedding force change continuously during the transport process. Therefore, this analysis can only describe the general laws of the quasi-static components varying with the parameters. In contrast, the non-monotonic responses of the impact force and the acceleration are dominated by dynamic mechanisms. These mechanisms include the randomness of the boulder impact, the formation and saturation of the buffer layer, and the transition of the impact mode from the distributed mode to the concentrated mode. These dynamic mechanisms exceed the descriptive capability of this theoretical framework. This is the main reason for the difference between the theoretical laws and the measured peak laws. Therefore, the theoretical results are applicable to trend judgment and parameter sensitivity analysis. For quantitative application, a dynamic model should be introduced and field verification should be carried out. Future work can further refine the analysis by combining numerical simulation and model tests. In addition, the dynamic response is also affected by factors such as the particle gradation of the debris mass, the inclination angle of the chute, and the impact scale. In summary, the boulder size and the distance in front of the slope jointly determine the dynamic response of the bridge pier under the impact of the dry granular flow. In engineering design, the optimization of a single factor should be avoided. A collaborative design considering both the particle gradation composition and the pier arrangement is recommended.

6. Conclusions

Based on typical cases of bridge collapse caused by dry granular flow, this study investigated the dynamic response of bridge piers under the impact of dry granular flow with giant boulders at different boulder sizes and pier-to-slope distances through physical model tests and PFC-FLAC coupled numerical simulations. The force mechanism of the giant boulders was theoretically analyzed. The main conclusions are as follows:

(1) Based on the physical model tests of dry granular flow with giant boulders impacting bridge piers, a PFC-FLAC coupled numerical analysis method was established. The numerical results were compared with the test results from two aspects, namely the peak acceleration response at the pier top and the macroscopic accumulation morphology. The results showed that the variation trends of the peak acceleration at the pier top obtained by the two methods are highly consistent. The accumulation range and the accumulation height in front of the pier were generally consistent. This indicates that the coupled numerical method can well simulate the dynamic process of dry granular flow with giant boulders impacting bridge piers, and it can provide reliable methodological support for subsequent parametric studies of boulder size.

(2) The boulder size and the distance in front of the slope have a significant influence on the impact force of dry granular flow, and the impact force in the X direction is much larger than that in the Y direction. With the increase in boulder size, the peak impact force of dry granular flow with giant boulders on the pier in the X direction first decreases and then increases. With the increase in the distance in front of the slope, the peak impact force first increases and then decreases, and the peak time is prolonged.

(3) The acceleration at the pier top under the impact of dry granular flow with giant boulders is significantly affected by the boulder size and the distance in front of the slope. The acceleration at the pier top increases with the increase in boulder size and decreases with the increase in the distance in front of the slope.

(4) The quasi-static theoretical force analysis of the giant boulders shows that the boulder size and the density are the key parameters controlling the forces acting on the giant boulders. The supporting force and the drag force of the dry granular flow on the giant boulders increase with the increase in the density of the dry granular flow, while the friction force decreases. The gravity and the supporting force acting on the giant boulders increase with the increase in boulder size.

(5) This study still has the following limitations: a 1:20 scaled model and a fixed chute with an inclination angle of 45° were adopted; only a single gradation of the debris mass and rectangular cross-section piers were considered; the result of each condition was obtained from a single test, making it difficult to evaluate the discreteness and confidence interval; independent numerical validation is lacking for the slope-toe-distance series, and the large-boulder conditions are numerical predictions; the force analysis is a quasi-static approximation. In future work, multi-batch repeated tests will be carried out to improve statistical significance; independent numerical simulations will be completed for the full slope-toe-distance series; physical model tests with large-diameter boulders will be progressively conducted; and the parameter analysis will be extended to the particle gradation, chute inclination, and impact scale, together with dynamic modeling and field verification, to improve the applicability of the model and the reliability of the conclusions.

Author Contributions: Conceptualization, M.C. and J.C.; methodology, M.C.; software, J.C. and P.T.; validation, J.C. and S.G.; formal analysis, J.C. and Y.Z.; investigation, J.C., P.T., S.G. and X.C.; resources, M.C.; data curation, X.C. and Y.Z.; writing—original draft preparation, J.C.; writing—review

and editing, M.C. and J.C.; visualization, S.G. and P.T.; supervision, M.C.; project administration, M.C.; funding acquisition, M.C. All authors have read and agreed to the published version of the manuscript.

Funding: The authors gratefully acknowledge the financial support provided by the National Natural Science Foundation of China (Grant No. 52368026), the Natural Science Basic Research Program of Shaanxi Province (Grant No. 2023-JC-YB-437).

Data Availability Statement: The original contributions presented in this study are included in the article. Further inquiries can be directed to the corresponding authors.

Conflicts of Interest: The authors declare no conflicts of interest.

References

1. Fan, X.; He, A.; Liu, H.; Xia, G.; Zhou, Y.; Chen, J. Study on the dynamic response of bridges in mountainous areas damaged by debris avalanche impact. *J. Vib. Shock* **2026**, *45*, 129–140. (In Chinese) [CrossRef]
2. Zhang, Z.D.; Fan, X.Y.; Jiang, Y.J. Study on the influence of grain sequence distribution in the source area and particle size on the impact action of debris avalanches. *Hydrogeol. Eng. Geol.* **2021**, *48*, 49–59. (In Chinese) [CrossRef]
3. He, S.; Liu, W.; Li, X. Prediction of impact force of debris flows based on distribution and size of particles. *Environ. Earth Sci.* **2016**, *75*, 298. [CrossRef]
4. Yang, C.; Zhang, S.; Yin, Y.; Yang, H.; Wei, F. Dynamic-based model for calculating the boulder impact force in debris flow. *J. Mt. Sci.* **2024**, *21*, 1930–1940. [CrossRef]
5. Si, G.W.; Chen, X.Q.; Chen, J.G.; Tang, J.B.; Zhao, W.Y.; Jin, K. The impact force of large boulders with irregular shape in flash flood and debris flow. *KSCE J. Civ. Eng.* **2022**, *26*, 4276–4289. [CrossRef]
6. Zhang, G.; He, C.; Jiang, L.Z.; Guo, W. Dynamic response and protection of RC piers under debris flow impact: An SPH-DEM-FEM coupled modeling approach. *Mech. Based Des. Struct. Mach.* **2026**, *54*, 2609991. [CrossRef]
7. Jiang, L.; Xiao, W.; Lai, Z.; Mou, B. Dynamic characteristics and impact load properties of high-speed railway piers under debris flow impact. *Transp. Geotech.* **2025**, *52*, 101562. [CrossRef]
8. Jin, Z.H.; Wei, F.F.; Wu, Y.W.; Qu, K.; Luo, X.; Ren, X. Simulations of debris flow impacting on bridge pier based on coupled CFD-DEM method. *Ocean Eng.* **2023**, *279*, 114532. [CrossRef]
9. Cheng, M.L.; Gao, W.W. Study on the impact law of V-shaped gully debris avalanches on double-column piers. *Buildings* **2024**, *14*, 577. [CrossRef]
10. Xing, L.; Wang, G.; Gong, W.; Xu, M.; Jaboyedoff, M.; Wang, F. Model tests of the failure behaviors of buildings under the impact of granular flow. *Landslides* **2025**, *22*, 373–392. [CrossRef]
11. Kim, B.J.; Yune, C.Y. Flume investigation of debris flow entrained boulders with cylindrical baffles and a rigid barrier. *Eng. Geol.* **2025**, *344*, 107836. [CrossRef]
12. Yu, X.; Liu, Y.; He, S.; Liu, W.; Guo, L.; Wu, Y.; Lyu, A.; Wang, D.; Liu, Y. Impact stress fluctuations and induced vibrations in granular flow–cylinder interactions: Insights from laboratory experiments. *Acta Geotech.* **2026**, *21*, 2239–2258. [CrossRef]
13. Zhu, Y.; Zhang, Y.; Ward, S.N.; Liu, Y.; Xiao, L.; Zheng, H.; Zhao, F. Topographic controls on kinematic characteristics of the 2015 Shanyang catastrophic landslide: Insights from field investigations and Tsunami Squares modeling. *Landslides* **2025**, *22*, 3801–3822. [CrossRef]
14. Liu, G.; Kang, J.; Zhong, Z.; Bo, W.; Fan, H.; Yang, C. Laboratory Experiments and 3D DDA Numerical Simulations on Rockfall Movement Characteristics. *Rock Mech. Rock Eng.* **2025**, *58*, 9747–9769. [CrossRef]
15. Cheng, M.L. Numerical analysis of the dynamic response of concrete bridge piers under the impact of rock debris flow. *Buildings* **2024**, *14*, 1504. [CrossRef]
16. Wang, Z.; Zhou, H.; Li, Y.; Wang, Z. Numerical Simulation of Debris Flow Impact on Pier With Different Cross-Sectional Shapes Based on Coupled CFD-DEM. *Int. J. Numer. Anal. Methods Geomech.* **2025**, *49*, 2025–2046. [CrossRef]
17. Wang, Y.; Liu, X.; Yao, C.; Li, Y.; Liu, S.; Zhang, X. Finite release of debris flows around round and square piers. *J. Hydraul. Eng.* **2018**, *144*, 06018015. [CrossRef]
18. Liang, J.J.; Zhu, K.Y. Protective mechanism of disaster prevention pile groups against rock avalanche impact on bridge piers. *J. Chengdu Univ. Technol. (Sci. Technol. Ed.)* 2026, *in press*. (In Chinese)
19. Tang, H.; Xia, C.; Wang, K.; Jiang, J.; Xia, H. Reliability-based vulnerability analysis of bridge pier subjected to debris flow impact. *Struct. Infrastruct. Eng.* **2024**, *20*, 1–12. [CrossRef]
20. Yao, C.; Xu, C.; Zhou, X.; Liu, Q.; Qiang, B. Study on the destruction process of piers by debris flow impact using SPH-FEM adaptive coupling method. *KSCE J. Civ. Eng.* **2024**, *28*, 3162–3175. [CrossRef]

21. Wang, Z.; Zhou, H. DEM investigation of the interaction between dry granular flow and pier with coupled particle size and Froude characteristics. *Granul. Matter* **2025**, *27*, 90. [CrossRef]
22. Liu, W.; Yan, S.; He, S.; Wang, D. Numerical study on the damage evaluation of a check dam under boulder-enriched debris flow impact. *Eng. Geol.* **2025**, *360*, 108479. [CrossRef]
23. Wang, D.; Chen, Z.; He, S.; Liu, Y.; Tang, H. Measuring and estimating the impact pressure of debris flows on bridge piers based on large-scale laboratory experiments. *Landslides* **2018**, *15*, 1331–1345. [CrossRef]
24. Jiang, Y.J.; Towhata, I. Experimental study of dry granular flow and impact behavior against a rigid retaining wall. *Rock Mech. Rock Eng.* **2013**, *46*, 713–729. [CrossRef]
25. Sun, H.; You, Y.; Liu, J.; Zhang, G.; Feng, T.; Wang, D. Experimental study on discharge process regulation to debris flow with open-type check dams. *Landslides* **2021**, *18*, 967–978. [CrossRef]
26. Wang, F.; Chen, Y.; Yan, K. A destructive mudstone landslide hit a high-speed railway on 15 September 2022 in Xining city, Qinghai province, China. *Landslides* **2023**, *20*, 871–874. [CrossRef]
27. D'Angelo, M.; Civera, M.; Giordano, P.F.; Borlenghi, P.; Ballio, F.; Limongelli, M.P.; Chiaia, B. Bridge collapses in Italy across the 21st century: Survey and statistical analysis. *Struct. Infrastruct. Eng.* **2025**, 1–23. [CrossRef]
28. Gabrieli, F.; Gibin, F.; Brezzi, L.; Mangraviti, V.; Cernuto, E.; Lupattelli, A.; Salciarini, D.; Mammoliti, E.; Dezi, F.; Stacul, S.; et al. Understanding landslide-bridge interactions through a comprehensive analysis of a global case study database. *Int. J. Bridge Eng. Manag. Res.* **2025**, *2*, 214250012. [CrossRef]
29. *GB 55008-2021*; General Code for Concrete Structures. China Architecture and Building Press: Beijing, China, 2021. (In Chinese)
30. *GB 50010-2010*; Code for Design of Concrete Structures. China Architecture & Building Press: Beijing, China, 2011. (In Chinese)
31. Zhang, H.Y.; Lin, C.K.; Zhuang, H.J.; Wang, G.Y. Similarity of the fire behavior of reinforced concrete columns exposed to fire on four sides and the influence of concrete spalling. *Eng. Mech.* 2026; *in press*. (In Chinese)
32. Luo, X.; Cao, P.; Liu, T.; Zhao, Q.; Meng, G.; Fan, Z.; Xie, W. Mechanical behaviour of anchored rock containing weak interlayer under uniaxial compression: Laboratory test and coupled DEM–FEM simulation. *Minerals* **2022**, *12*, 492. [CrossRef]
33. Chen, Y.; Wu, J.L.; Wu, K.; Huang, X.; Li, C.H. Seismic response analysis of deep-water bridge piers considering pile-soil interaction. *Eng. Mech.* **2024**, *41*, 176–184. (In Chinese) [CrossRef]
34. Wang, Q.; Chen, J.; Wang, H.; Zhang, Q. Impact force of boulders conveyed in debris flows on bridge piers and collision protection measures. *Int. J. Geohazards Environ.* **2016**, *2*, 72–81. [CrossRef]

Disclaimer/Publisher's Note: The statements, opinions and data contained in all publications are solely those of the individual author(s) and contributor(s) and not of MDPI and/or the editor(s). MDPI and/or the editor(s) disclaim responsibility for any injury to people or property resulting from any ideas, methods, instructions or products referred to in the content.